Journal of Materials Science & Technology 58 (2020) 114–119

Contents lists available at ScienceDirect

Journal of Materials Science & Technology

journal homepage: www.jmst.org

Research Article

In-situ study of initiation and extension of nano-thick defect-free channels in irradiated nickel

Shihao Li [a,b], Ning Gao [c,d,**], Weizhong Han [a,*]

[a] Center for Advancing Materials Performance from the Nanoscale, State Key Laboratory for Mechanical Behavior of Materials, Xi'an Jiaotong University, Xi'an, 710049, PR China
[b] School of Materials Science and Engineering, Zhengzhou University, Zhengzhou, 450001, PR China
[c] Institute of Frontier and Interdisciplinary Science and Key Laboratory of Particle Physics and Particle Irradiation, Shandong University, Qingdao, 266237, PR China
[d] Institute of Modern Physics, Chinese Academy of Sciences, Lanzhou, 730000, PR China

ARTICLE INFO

Article history:
Received 5 February 2020
Received in revised form 10 March 2020
Accepted 20 March 2020
Available online 11 June 2020

Keywords:
Defect-free channel
Dislocation loop
In-situ
Strain localization

ABSTRACT

Radiation defects-induced plastic flow localization is the origin of loss of ductility in irradiated metals. Defect-free channels (DFCs) are a typical form of strain localization that lead to crack initiation and premature failure. A comprehensive understanding of the DFC dynamics is key to managing radiation boosted property degradation. Despite great research efforts, a clear mechanism of DFC remains unknown. Here, our in-situ tests on irradiated Ni pillars provide a real-time observation of the dynamics of DFCs, including DFC initiation, extension and thickening. The merging and spreading of dislocation loops serve as an alternative mechanism of dislocation sources that emit massive dislocations and initiate nano-thick DFCs inside the grain. Nano-thick DFCs were formed through chopping up or sweeping away of loops by mobile dislocations. Annihilation of opposite loops and interactions between loops and vacancies accelerate DFC extension. Activation of multiple dislocation sources and dislocation cross-slips are the mechanisms for DFC thickening.

1. Introduction

Energetic particle irradiation causes significant degradation of the mechanical properties of metals, most notably an increase in yield stress and decrease in ductility, often accompanied by plastic flow localization [1–6]. Plastic flow localization in the form of defect-free channels (DFCs, also named dislocation-free channels), which appear to be free of radiation-produced defects, causes loss of ductility and premature failure [6–20]. Although the existence of DFCs in various metals is well established [6–20], the understanding of dynamic processes for DFC initiation, extension and interaction with other defects is far from complete.

Extensive experimental and simulation efforts have attempted to shed light on the mechanisms that lead to irradiation-induced strain localization [6–20]. In general, DFCs distributed along slip planes are free of radiation defects and act as pathways for localized plastic flow because of low defect density. High strain concentration along DFCs causes deformation localization and stress concentration at the grain boundaries, which further triggers intergranular cracking [12–14]. The movement of dislocations may sweep away, absorb or destroy radiation defects, which are responsible for DFC formation and localization of strain [6–20]. However, the answers to a few critical questions regarding the dynamics of DFC remain unclear. First, where are the favorite nucleation sites for DFCs? Second, is it possible to produce a DFC from the grain interior, especially one initiated from those radiation defects [16]? Third, what are the dynamic formation processes of DFC under uniaxial loading? Because of the lack of quantitative in-situ investigations, a clear picture of the dynamic formation of DFCs is missing. DFCs were proposed to originate from grain boundaries or from the vicinity of crack tip, and no dislocation sources were observed to operate within a grain [21,22]. A dynamic observation of DFC evolution could provide details of DFC initiation, extension and thickening.

* Corresponding author at: Center for Advancing Materials Performance from the Nanoscale, State Key Laboratory for Mechanical Behavior of Materials, Xi'an Jiaotong University, Xi'an, 710049, PR China.
** Corresponding author at: Institute of Frontier and Interdisciplinary Science and Key Laboratory of Particle Physics and Particle Irradiation, Shandong University, Qingdao, 266237, PR China.
E-mail addresses: wzhanxjtu@mail.xjtu.edu.cn (W. Han), ning.gao@sdu.edu.cn (N. Gao) .

https://doi.org/10.1016/j.jmst.2020.03.057
1005-0302/

Because of the limitations of experimental methods and difficulties in simulating high-density radiation defects [11–16], uncovering these essential details about the collective physical processes of DFC dynamics remains challenging.

In this study, we performed in-situ tensile tests on self-ion irradiated Ni pillars with high dislocation loops density to capture the dynamic formation processes of nano-thick DFCs under straining. The experiments provide a direct, real-time observation of the DFC formation processes, including DFC initiation, extension and thickening. The merging and spreading of dislocation loops play important roles in producing massive mobile dislocation sources inside the grain, which further initiate nano-thick DFCs. Nano-thick DFCs were formed because of chopping up or sweeping away of loops by mobile dislocations.

2. Materials and methods

Ni single crystal foils with size of 10 mm (length) × 10 mm (width) × 0.2 mm (thickness) were purchased commercially and used as model materials in this study. The Ni thin foils were irradiated using 350 MeV self-ions at -60 to -40 °C. To achieve a uniform radiation damage profile across the implanted region, the incident Ni ions were designed to pass through an energy degrader that comprised 10 Al foils of various thicknesses before reaching the free surface of sample [23,24]. The average radiation damage is 0.5 dpa (displacement per atom) and the thickness of irradiated region is around 23 μm. The samples were then machined using focused ion beam (FIB) to perform initial microstructural characterization and in-situ mechanical testing inside a transmission electron microscope (TEM). In order to minimize the FIB induced damage, we performed very carefully polishing during the last step of FIB machining using low voltage (5 kV) and beam current (47 pA). All pillars for in-situ tensile tests were fabricated by FIB micromachining. To eliminate size effect, pillars were design to have a similar size of 1 μm in gauge length, 400 nm in width and 150 nm to 200 nm in thickness. In-situ tensile tests were conducted using Hysitron PicoIndentor (PI 95) under displacement control mode with a strain rate of about 1×10^{-3} s^{-1} inside a JOEL 2100 TEM. The dislocation loop density of as-irradiated Ni was determined by counting the number of dislocation loops in regions with size of 200 nm × 200 nm × 120 nm (sample thickness) and averaged.

3. Results

Figs. 1a and b show bright field and dark field TEM images of radiation defects in irradiated Ni. High density of dislocation loops with an average diameter of 4.1 nm formed homogeneously after self-ion irradiation. These dislocation loops are clustered and aligned along the $\{110\}_{Ni}$. The ordered dislocation loops are frequently observed in other irradiated metals as well [23–30]. Fig. 1c highlights the isolated dislocation loops. As marked by the yellow arrows, some tiny isolated dislocation loops other than those in queue can be identified. The dislocation loop density is about 3×10^{22} m^{-3}. There are several types of dislocation loops according to the imaging vectors, including loops with Burgers vectors of 1/2 < 110> and 1/3 < 111 > . Almost no line dislocations can be found in the as-irradiated sample. We also performed microstructural characterization on unirradiated Ni samples fabricated using FIB lift out to evaluate FIB-induced damages. Low-density dispersed dislocation loops were observed in unirradiated Ni, which indicates that self-ion irradiation induced dislocation loops are the main defects in Ni pillars.

Fig. 2 shows in-situ deformation processes of a small-volume Ni pillar with high dislocation loops density and loaded along [335] zone axis. Frequent strain bursts appear on the stress-strain curves during straining (Fig. 2a and Movie S1), which indicate that the plastic instability is due to dislocation-loop interactions [16,31]. The critical resolved shear stress for strain bursts is around 327 MPa. Obvious hardening can be identified before some strain bursts, as marked by the blue arrows in Fig. 2a. The magnitude of hardening is around 100 to 200 MPa, which is due to obstruction of dislocations by radiation defects [22]. Figs. 2b-e show dark field snapshots of the microstructures of samples after a series of strain bursts, as labeled in Fig. 2a. DFC nucleation was triggered at low plastic strain and just after the first strain burst, as manifested by the nano-thick DFC embryos in the lower part of the pillar in Fig. 2b. Most of the DFC embryos are in the interior of the sample rather than initiate from the edges. These channel embryos are similar to the "packets of channels" observed in irradiated Mo just after macroscopic yielding but the DFCs here are much shorter [16]. With further straining, these embryos propagate toward two ends and gradually develop into nano-thick DFCs across the whole sample (Fig. 2c). One nano-thick DFC grows from the center while its two ends are still inside the sample, as marked by the yellow arrows in Fig. 2c. Further tensile deformation rapidly accelerates DFC extension in the irradiated Ni pillar and these form a DFC-dominated region, as labeled by the white dashed contour in Fig. 2d. All these DFCs are parallel to the (111) plane. With further loading, the stress gradually increased again in the sample, as marked by e in Fig. 2a. Once the stress reached around 900 MPa, a big strain burst occurred, and deformation was localized in a few major DFCs, accompanied by DFC thickening, as indicated by the black channel in the sample and large slip offset left at sample edges (Fig. 2e). The current real-time observations of deformation in irradiated Ni pillar uncover the dynamics of DFCs, including channel initiation, extension and thickening, which correspond to different degree of plastic flow localization. The initiation, extension and thickening of DFC are correlated with the strain bursts on the engineering stress-strain curves.

Next, we address the detailed DFC nucleation processes. As a major radiation defect in the current sample, dislocation loops play an important role in DFC formation. Fig. 3 and Movie S2 show the dynamic evolution of dislocation loops and dislocation-loop interactions under straining. Before the tensile test, numerous ordered dislocation loops are distributed uniformly across the sample. Under straining, some of the dislocation loops can slip or migrate and approach each other. Figs. 3a and b show an example of the merging of two loop clusters into a new crescent loop group. Surprisingly, with further straining, the upper part of the new dislocation loop cluster evolves into a short curved line dislocation via a loop reaction (green arrow in Fig. 3c), while the lower part remained as a dislocation loop cluster (yellow arrow in Fig. 3c). Dislocation loop migration here is different from loop "diffusion" with the aid of stochastic thermal fluctuation at elevated temperature [32]. Instead, loops move through loop glide on their cylinders or slip plane [16,33]. The formation of a curved line dislocation creates dislocation sources inside the forest of dislocation loops. Under straining, the curved line dislocation can repeatedly bow out mobile dislocations. This mechanism provides a chance to create DFCs from the grain interior rather than from grain boundaries [22]. The nucleation of mobile dislocations from helium bubbles has been observed experimentally [34], while the producing line dislocation via loop coalescence remains as a proposal [16]. The current observation provides direct experimental evidence on line dislocation production through loop aggregation and reaction. Therefore, the transformation of dislocation loops into line dislocation serves as an alternative formation mechanism of mobile dislocation sources to initiate DFC. This observation is consistent with Movie S1 in which dislocation loops migrate at the early stage of deformation under low flow stress. Subsequently, active dislocation movements are

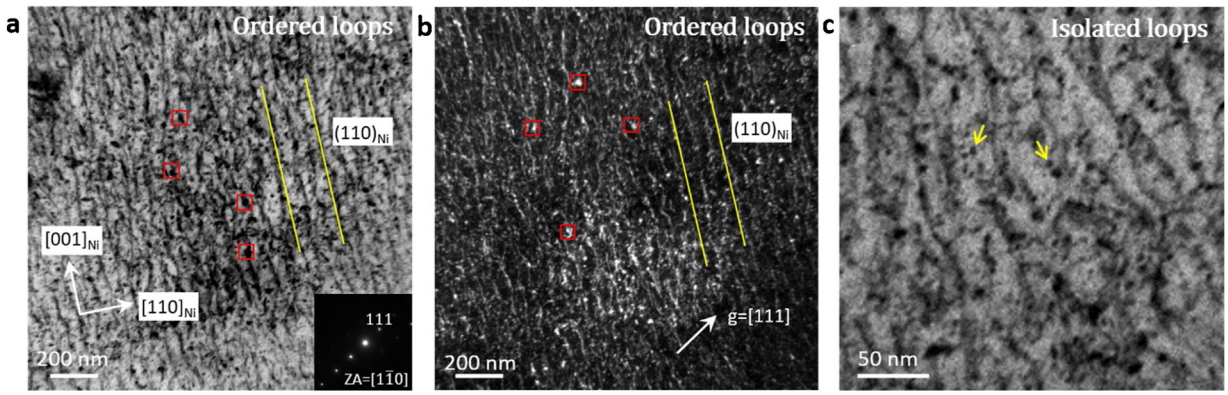

Fig. 1. Ordered dislocation loops in irradiated Ni. (a) Bright field and (b) dark field image of dislocation loops. Ordered dislocation loops are aligned roughly along the (110) plane. (c) Highlight of isolated dislocation loops with an average size of 4.1 nm.

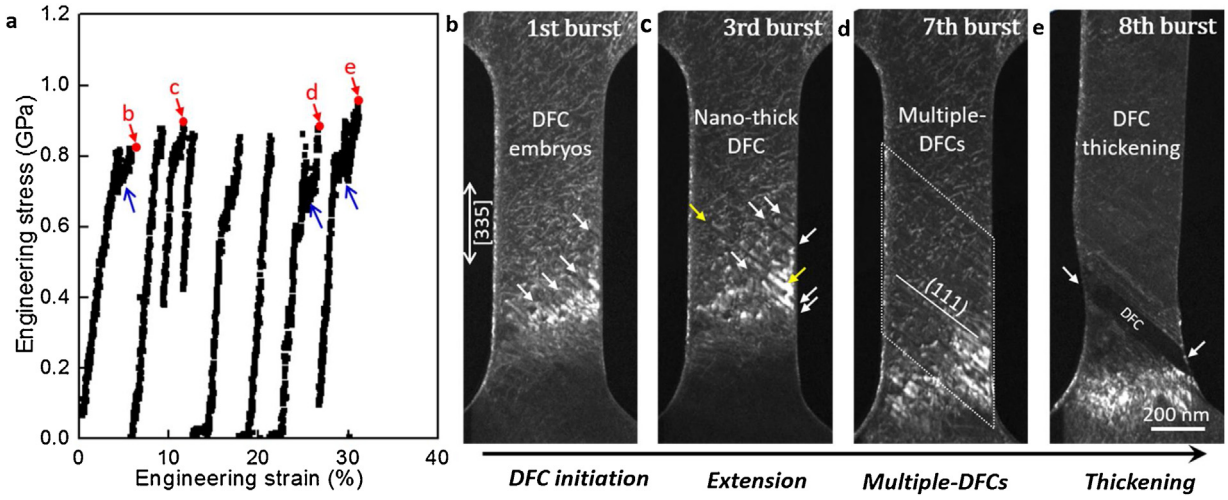

Fig. 2. Microstructural evolution in tensile of small-volume Ni along [335]. (a) Frequent strain bursts in the stress-strain curve. (b)-(e) Dark field images showing evolution of DFCs under straining. (b) DFC nucleation, (c) DFC growth, (d) multiple DFC propagation and (e) DFC thickening.

observed inside the sample before DFC embryo formation and the first strain burst.

After nucleation of mobile dislocation sources, the following dislocation-loop interactions are key to DFC initiation. Figs. 3d-f and Movie S3 show the processes of cleaning of two dislocation loops and pinning of mobile dislocations (labelled as 1 and 2) by loops. With the proceeding load, the two line dislocations move toward the lower left part of the sample and encounter two dislocation loops next to each other (marked by yellow arrows). Dislocation 1, which shares a slip path with dislocation 2, was pinned by the two dislocation loops located on its slip plane. The inset shows TEM images of dislocations and dislocation loops in higher magnification. With gradually increasing strain, dislocation 1 was fixed at the pinning position without motion, while dislocation 2 continued to move slowly towards dislocation 1 (Movie S3). Once a critical distance of 1–2 nm was reached, dislocation 1 moved suddenly in the initial slip direction, accompanied by the synchronous slip of dislocation 2. This phenomenon shows that dislocation 2 exerted an additional stress on dislocation 1; thus a dislocation pile-up took place and the higher accumulated stress promoted the depinning of dislocation 1. According to Movie S3, dislocation 2 exceeded dislocation 1 at the moment of depinning, which likely corresponds to a cross-slip event, as marked in Figs. 3e and f. Notably, as labeled by the yellow dashed contours in Fig. 3e, two dislocation loops disappeared after the slip of dislocations 1 and 2, which left a defect-free region. The disappearance of dislocation loops has several possibilities. It can either be annihilated with opposite loops [11,16], swept away/absorbed by mobile dislocations [12–22] or recombined with radiation induced vacancies (frozen in place after irradiation) under the pushing of mobile dislocations. This results provide direct experimental evidence that irradiation-induced dislocation loops could be swept away/absorbed/annihilated during the slither of dislocations [12–22]. With further tensile deformation, dislocation 1 and dislocation 2 were once again pinned by other dislocation loops and delivered an inconsecutive and jerky slip with short mean free path (Fig. 3f and Movie S3). The stick-slip movement of dislocations led to the tiny drop and subsequent increase of stress on the stress-strain curves (Fig. 2a). Through the continuous pinning-depinning process, irradiation-induced dislocation loops were gradually chopped up or swept away by line dislocations or annihilated with radiation produced vacancies. All of these contribute to the initiation and extension of DFCs in irradiated Ni pillars.

Another interesting question is whether DFCs have a true clean passage? To answer this, we investigated the defect structures inside a well-developed DFC (Fig. 4). Before loading, regular dislocation loop clusters were distributed along the $\{110\}_{Ni}$ in as-fabricated samples (inset in Fig. 4a). Figs. 4a and b show dark field and bright field TEM images of a deformed Ni pillar. After loading, profuse parallel nano-thick DFCs along $(111)_{Ni}$ were formed (Fig. 4a; taken under the [1 $\bar{1}$ 0] zone axis with g=[111]). The average DFCs width in this sample is only 5.5 nm, which is close to the

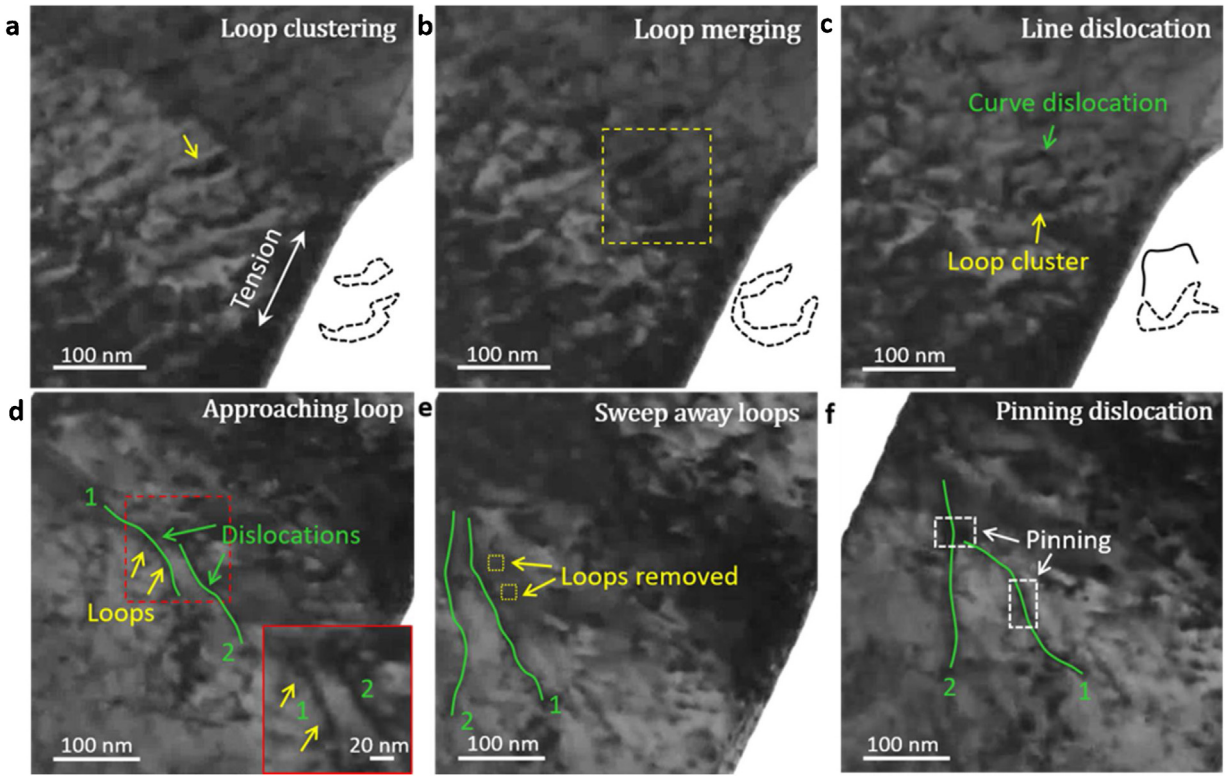

Fig. 3. Line dislocation formation and sweep away. (a)-(c) Dislocation loops migrate, interact and merge into line dislocations. (d)-(f) Interactions of line dislocations and dislocation loops under straining: pinning of line dislocation, cleaning of dislocation loops and cross-slip of dislocation 2 because of pile-up.

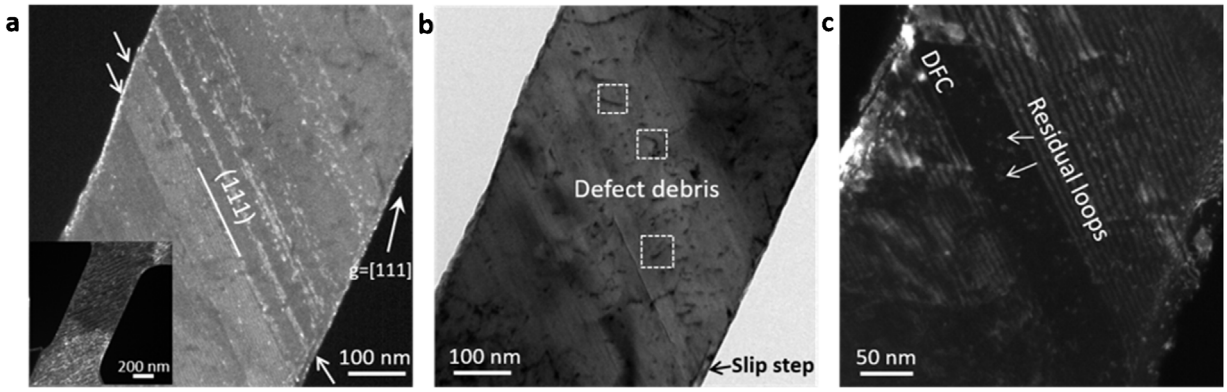

Fig. 4. Microstructures inside DFC. (a) Ultrathin DFC lines along (111) after loading. The inset shows the ordered loops before loading. (b) Dislocation debris inside DFC and slip steps at edge. (c) Dark field image of DFC from sample in Fig. 2.

lower limit of DFCs formed in bulk samples [10–16,35–38]. DFC formation was accompanied by severe localized deformation, as indicated by the sharp slip steps formed at the sample edges shown in Figs. 4a and b. Fig. 4c shows a dark-field TEM image taken under the [1 $\bar{1}$ 0] zone axis with g=[111] in another Ni pillar with one major DFC. Actually, the DFC is not completely free of defects, while much dislocation debris and some loop clusters are scattered inside the channel (Figs. 4b and c). Dislocation debris may stem from jogged dislocations resulting from dislocation-loop interactions [17,39], which can be active mobile dislocation sources for further localized plasticity. Additionally, this residual defect debris also serves as an obstacle for dislocation motion and enhances the possibility of dislocation cross-slip (Movie S3), thus causing DFC thickening [12,14].

4. Discussion

Our in situ tests demonstrate the entire DFC dynamics under straining, which include DFC initiation, extension and thickening. Fig. 5 summarizes the key steps for the dynamics of DFC formation. At the early stage of deformation, dislocation loops migrate, interact and merge into larger dislocation loops [16,33], accompanied by reduction of loop density. These large loops then broke and transformed into mobile dislocations (Fig. 5a). Subsequently, dislocation loops obstruct mobile dislocations [35], and the following pile-up of dislocations finally destroy/clean the loops along the dislocation passage via a stick-to-slip movement (Fig. 5b). This process resulted in a sharp decrease of loop density and promoted DFC nucleation and extension. Finally, DFC thickening was occasionally captured at the final deformation stage, which is related

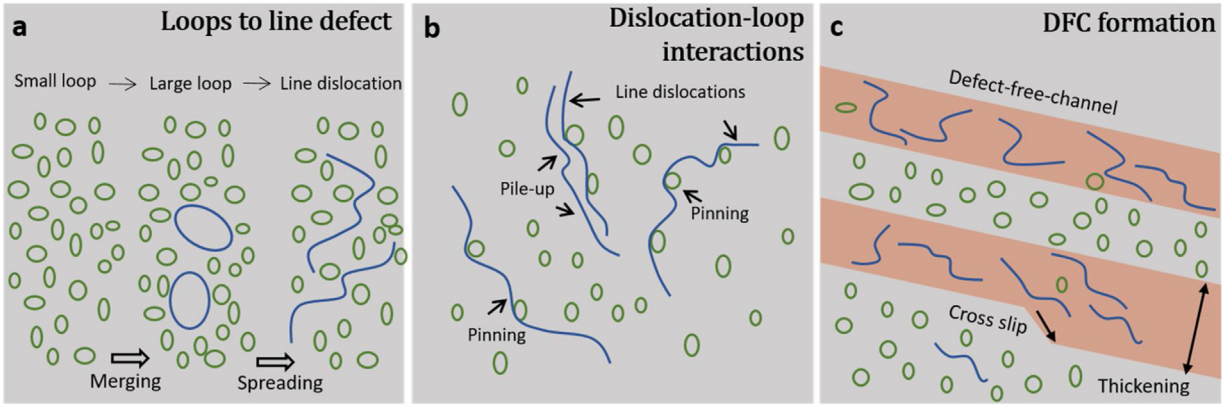

Fig. 5. Cartoon of the formation mechanism of DFC. (a) Nucleation of line dislocation by loops merging and spreading. (b) Pining of line dislocations by loops. (c) Cleaning of loops by line dislocation to form DFCs and thickening of DFCs by multiple dislocation sources operation and dislocation cross-slip.

to activation of multiple dislocation sources and residual defect debris induced dislocation cross-slip (Fig. 5c) [12,14]. Surface dislocation nucleation should also be possible in the deformation of small-volume metal and participate in the DFC thickening. However, considering the high density of easy glide dislocation sources inside the sample (profuse irradiation dislocation loops), we think that dislocations originating from internal dislocation sources play a dominate role in the formation and thickening of DFCs. As shown in Fig. 2a and Movie S1, the DFC is initiated in the interior of sample rather than starting from the edge of the sample, which indicate that the internal dislocation sources start first. One key observation here is that dislocation loop interactions directly give rise to mobile dislocation sources, which means the DFC can initiated from the grain interior and does not necessarily rely on grain boundary sources [21]. There are several ways for dislocation loops to evolve into line dislocation, for example, stress or thermal driven loop reconfigurations [33,39,40]. In this regard, dislocation loop coalescence and merging under external stress is a precursor for DFC initiation in irradiated Ni pillars [16]. The formation of only nano-thick DFCs in the current study is for the following reasons. First, the initial channel width is highly dependent on defect size [17]. Once mobile dislocations encountered defects, dislocations absorb the defects and jog up or down by a distance equal to half of the defect diameter [17]. Consequently, the initial DFC width is comparable with the mean defect size, which is only 4.1 nm in this case. Second, two main DFC widening methods, source widening [17,21] and dislocation cross-slip [6,11], were suppressed in nanoscale Ni pillars. Source widening triggers dislocation motion along adjacent planes, which leads to channel widening [17,21]. In this case, the merging and spreading of dislocation loops serve as a dislocation nucleation mechanism. Simultaneously formation of parallel dislocation sources are difficult in small-volume Ni. While the randomly distributed dislocations sources form via loop interactions (Fig. 3 and Movie S2), which create separated ultrathin DFCs. Additionally, mobile dislocations in nanoscale Ni pillars only can glide a short distance before disappearing at the free surface, which reduces the possibility of dislocation cross-slip. Therefore, the DFC width decreases with decreasing sample size [11]. Most dislocations glided along their initial slip paths without obvious signs of cross-slip (Fig. 3 and Movie S3). Notably, dislocation cross-slip may happen occasionally in well-developed channels because of the obstruction by residual defects, which causes channel thickening (Fig. 4d and Movie S3).

5. Conclusion

We demonstrate that the dynamic formation processes of DFCs under straining in self-ion irradiated Ni pillars. DFC formation includes initiation, extension and thickening. The merging and spreading of dislocation loops serve as an important mechanism for nucleation of active dislocation sources, which emit massive mobile dislocations and initiate nano-thick DFCs in the grain interior. Nano-thick DFCs were formed via chopping up or sweeping away of loops by mobile dislocations. Activation of multiple dislocation sources and dislocation cross-slips are the mechanism for DFC thickening in the final stage. These observations are beneficial to understand the dynamics of radiation defects and design of radiation tolerant materials.

Declaration of Competing Interest

The authors declare that they have no conflict of interest.

Acknowledgements

This work was supported by the National Natural Science Foundation of China (Grant Nos. 51922082, 51971170, 51942104 and 11675230), the National Key Research and Development Program of China (2017YFB0702301) and the 111 Project of China (Grant Number BP2018008).

Appendix A. Supplementary data

Supplementary material related to this article can be found, in the online version, at doi:https://doi.org/10.1016/j.jmst.2020.03.057.

References

[1] N. Hashimoto, T.S. Byun, K. Farrell, S.J. Zinkle, J. Nucl. Mater. 329 (2004) 947–952.
[2] G.E. Lucas, J. Nucl. Mater. 206 (1993) 287–305.
[3] D. Kiener, P. Hosemann, S.A. Maloy, A.M. Minor, Nature Mater. 10 (2011) 608–613.
[4] M.S. Ding, L. Tian, W.Z. Han, J. Li, E. Ma, Z.W. Shan,Phys. Rev. Lett. 117 (2016), 215501.
[5] X.H. Zhang, K. Hattar, Y.X. Chen, L. Shao, J. Li, C. Sun, K.Y. Yu, N. Li, M.L. Taheri, H.Y. Wang, J. Wang, M. Nastasi, Prog. Mater. Sci. 96 (2018) 217–321.
[6] T.D. De La Rubia, H.M. Zbib, T.A. Khraishi, B.D. Wirth, M. Victoria, M.J. Caturla, Nature 406 (2000) 871–874.
[7] Y. Dai, M. Victoria, MRS Symp. Proc. 439 (1997) 319–324.
[8] R.P. Tucher, M.S. Wechsler, S.M. Ohr, J. Appl. Phys. 40 (1969) 400–408.
[9] Y. Fan, Y.N. Osetskiy, S. Yip, B. Yildiz, Proc. Natl. Acad. Sci. 110 (2013) 17756–17761.
[10] F. Onimus, J.L. Bechade, D. Gilbon, Metall. Mater. Trans. A 44 (2013) 45–60.
[11] A. Arsenlis, M. Rhee, G. Hommes, R. Cook, J. Marian, Acta Mater. 60 (2012) 3748–3757.
[12] Y.N. Cui, G. Po, N. Ghoniem,Phys. Rev. Lett. 120 (2018), 215501.
[13] R.D. Carter, M. Atzmon, G.S. Was, MRS Symp. Proc. 373 (1995) 171–176.
[14] T.A. Khraishi, H.M. Zbib, T.D. De La Rubia, M. Victoria, Metall. Mater. Trans. B 33 (2002) 285–296.

[15] J. Zhao, J.T. Busby, G.S. Was, J. Nucl. Mater. 361 (2007) 218–227.
[16] S. Mahajan, B.L. Eyre, Acta Mater. 122 (2017) 259–265.
[17] P.J. Doyle, K.M. Benensky, S.J. Zinkle, J. Nucl. Mater. 499 (2018) 47–64.
[18] D.S. Li, H. Zbib, H. Garmestani, X. Sun, M. Khaleel, Comput. Mater. Sci. 50 (2011) 2496–2501.
[19] D. Terentyev, G. Monnet, P. Grigorev, Scr. Mater. 69 (2013) 578–581.
[20] X.J. Shi, L. Dupuy, B. Devincre, D. Terentyev, L. Vincent, J. Nucl. Mater. 460 (2015) 37–43.
[21] J. Kacher, G.S. Liu, I.M. Robertson, Micron 43 (2012) 1099–1107.
[22] J.S. Robach, I.M. Robertson, B.D. Wirth, A. Arsenlis, Philos. Mag. 83 (2003) 955–967.
[23] C.H. Zhang, Y.T. Yang, Y. Song, J. Chen, L.Q. Zhang, J. Jang, A. Kimura, J. Nucl. Mater. 455 (2014) 61–67.
[24] Z.N. Ding, C.H. Zhang, Y.T. Yang, Y. Song, A. Kimura, J. Jang, J. Nucl. Mater. 493 (2017) 53–61.
[25] W. Jäger, P. Ehrhart, W. Schilling, F. Dworschak, A.A. Gadalla, N. Tsukuda, Mater. Sci. Forum. 82 (1986) 265–270.
[26] V.K. Sikka, J. Moteff, J. Nucl. Mater. 46 (1973) 217–219.
[27] S.L. Dudarev, K. Arakawa, X. Yi, Z. Yao, M.L. Jenkins, M.R. Gilbert, P.M. Derlet, J. Nucl. Mater. 455 (2014) 16–20.
[28] R.S. Barnes, D.J. Mazey, Acta Metall. 11 (1963) 281–286.
[29] X. Yi, M.L. Jenkins, K. Hattar, Acta Mater. 92 (2015) 163–177.
[30] M. Eldrup, B.N. Singh, S.J. Zinkle, T.S. Byun, K. Farrell, J. Nucl. Mater. 307 (2002) 912–917.
[31] Y.M. Yang, H. Abe, N. Sekimura, Phys. Lett. A 315 (2003) 293–300.
[32] K. Arakawa, K. Ono, M. Isshiki, K. Mimura, M. Uchikoshi, H. Mori, Science 318 (2007) 956–959.
[33] K. Arakawa, T. Amino, H. Mori, Acta Mater. 29 (2011) 141–145.
[34] M.S. Ding, J.P. Du, L. Wan, S. Ogata, L. Tian, E. Ma, W.Z. Han, J. Li, Z.W. Shan, Nano Lett. 16 (2016) 4118–4124.
[35] M. Briceño, J. Fenske, M. Dadfarnia, P. Sofronis, I.M. Robertson, J. Nucl. Mater. 409 (2011) 18–26.
[36] B.N. Singh, A. Horsewell, P. Toft, J. Nucl. Mater. 271 (1999) 97–101.
[37] A. Patra, D.L. McDowell, Acta Mater. 110 (2016) 364–376.
[38] S.J. Zinkle, B.N. Singh, J. Nucl. Mater. 351 (2006) 269–284.
[39] C. Erel, G. Po, T. Crosby, N. Ghoniem, Comput. Mater. Sci. 140 (2017) 32–46.
[40] Y. Chen, K. Murakami, H. Abe, Z.C. Li, N. Sekimura, Acta Mater. 163 (2019) 78–90.